Modeling Beam-Driven and Laser-Driven Plasma Wakefield Accelerators with XOOPIC

David L. Bruhwiler,[a] Rodolfo Giacone,[b] John R. Cary,[a,b] John P. Verboncoeur,[c] Peter Mardahl,[c] Eric Esarey[d] and Wim Leemans[d]

[a] *Tech-X Corporation, 5541 Central Avenue, Suite 135, Boulder CO 80301, USA*
[b] *University of Colorado at Boulder, Physics Department, Boulder CO 80309-0390, USA*
[c] *University of California Berkeley, EECS Department, Berkeley CA 94720-1770, USA*
[d] *Lawrence Berkeley National Laboratory, University of California, Berkeley CA 94720, USA*

Abstract. We present 2-D particle-in-cell simulations of both beam-driven and laser-driven plasma wakefield accelerators, using the object-oriented code XOOPIC, which is time explicit, fully electromagnetic, and capable of running on massively parallel supercomputers. Simulations of laser-driven wakefields with low (~10^{16} W/cm^2) and high (~10^{18} W/cm^2) peak intensity laser pulses are conducted in slab geometry, showing agreement with theory. Simulations of the E-157 beam wakefield experiment at the Stanford Linear Accelerator Center, in which a 30 GeV electron beam passes through 1 m of preionized lithium plasma, are conducted in cylindrical geometry, obtaining good agreement with previous work. We briefly describe some of the more significant modifications to XOOPIC required by this work, and summarize the issues relevant to modeling electron-neutral collisions in a particle-in-cell code.

INTRODUCTION

The quest to understand the fundamental nature of matter requires ever higher energy particle collisions, which in turn leads to ever larger and more expensive particle accelerators. Plasma-based accelerators can sustain electron plasma waves (EPW) with longitudinal electric fields on the order of the nonrelativistic wave breaking field, $E_0=cm_e\omega_p/e$, where $\omega_p=(4\pi n_e e^2/m_e)^{1/2}$ is the plasma frequency at an electron density n_e (see Ref. 1 for a review). For $n_e=10^{18}$ cm^{-3}, the electric field is $E_0\cong 100$ GV/m, with a phase velocity close to the speed of light. Laser plasma accelerators have demonstrated accelerating gradients of 100 GV/m -- several orders of magnitude higher than for conventional structures -- providing hope for reaching new energy regimes. Such large amplitude plasma wakefields can also be driven by intense relativistic particle beams.

Laser-Driven Plasma Wakefield Acceleration (LWFA)

Research in laser plasma acceleration is very active, with many innovative concepts being explored through theory[2-9] and experiment.[10-16] In the "standard" laser wakefield accelerator (LWFA) concept,[1] a single short (<1ps), ultrahigh intensity (>10^{18}

W/cm^2) laser pulse injected into an underdense plasma excites an EPW behind the pulse. The plasma wake is excited by the ponderomotive force created by rapid oscillations of the electromagnetic field. The wakefield amplitude is maximum when the laser pulse length L is approximately equal to the plasma wavelength $L=\lambda_p$, where $\lambda_p=2\pi c/\omega_p$. A correctly placed trailing electron bunch can be accelerated by the axial electric field and focused by the transverse electric field of the plasma wake.

Both 2-D and 3-D LWFA simulations are extremely demanding computationally, due to multiple time and space scales. The multiple scales arise, because the laser radiation field and the transverse electron oscillations evolve on a short time scale -- governed by the laser frequency ω -- with a correspondingly short wavelength, while the longitudinal plasma dynamics and consequent particle acceleration evolve on a much longer time scale -- governed by the electron plasma frequency ω_p -- and longer wavelength. Depending on the density of the plasma, the ratio ω/ω_p can vary from order unity to as high as 100. Thus, simulation codes for these problems must be parallelizable, so they can run on massively parallel processors (MPP), and they must also implement a "moving window" algorithm to follow the laser pulse over distances long compared to the pulse length.

A particle-in-cell (PIC) treatment of laser plasma acceleration[17-20] provides the most detailed simulation of the relevant physics, but is generally constrained to follow the short time scale evolution of the laser pulse, and thus is the most computationally expensive approach. Fluid treatments[21-23] are computationally more efficient, especially models that average over the faster time scales, and are less noisy than PIC, but cannot model the dynamics of accelerated electrons. A third approach[24] uses a PIC treatment of time-averaged equations, along with the use of the quasistatic approximation[25] and sometimes other assumptions. Quasistatic approximations impose the assumption that there is a single forward-propagating laser pulse, thus ruling out certain instabilities, as well as all accelerating concepts involving multiple laser pulses that are incident from various angles.

Beam-Driven Plasma Wakefield Acceleration (PWFA)

Beam-driven plasma wakefield accelerators (PWFA)[26,27] are also capable of providing dramatic accelerating gradients, and thus may lead to a next-generation of smaller, cheaper high-energy accelerators. The acceleration mechanism in the PWFA is analogous to that in the LWFA, only in the PWFA the EPW is excited by the space charge force of the drive bunch, as opposed to the ponderomotive force of the laser pulse. It has been proposed[28] to use the PWFA concept as a means of doubling the beam energy of the Stanford Linear Accelerator Center (SLAC) Linear Collider (SLC) in a distance of only seven meters. This so called “afterburner” would possibly enable detection of the Higgs particle.

A PWFA experiment, referred to as the E-157 experiment,[29-33] aimed at demonstrating accelerating gradients on the order of 1 GeV/m is currently underway at SLAC. In this experiment, a 30 GeV electron bunch is injected into a 1 to 1.5 m long plasma column with density on the order of 2-3 x 10^{14} cm^{-3}. E-157 operates in the “blow-out” regime of the PWFA, meaning the number density of the electron bunch is greater than the plasma density, so that all of the plasma electrons are expelled from

the axis in the vicinity of the electron bunch. The EPW generated by the electron bunch is expected to accelerate electrons in the tail of the bunch to higher energies. The plasma afterburner concept is a scaled up version of E-157, which will operate at much higher plasma density, thus requiring a much short duration electron bunch, which will generate an EPW with much stronger longitudinal fields.

In E-157, the laser-ionized lithium plasma density is roughly 10% of the neutral lithium density, $n_0 \sim 2 \times 10^{15}$ cm^{-3}. One proposal for an SLC afterburner[28] requires a plasma density two orders of magnitude larger, corresponding to a neutral lithium density of $n_0 \sim 2 \times 10^{17}$ cm^{-3}. At such high densities, the effects of electron-neutral collisions could modify the physics of the EPW.

The XOOPIC Particle-in-Cell Code

The standard PIC scheme[34] solves the equations representing a coupled system of charged particles and fields. The particles are followed in a continuum space, while the fields are computed on a mesh. First, forces due to the electric and magnetic fields are used to advance the velocities of the particles, and subsequently the velocity is used to advance the position. Particle boundary conditions such as emission and absorption are then applied. If collisions with a neutral background gas are included, the velocities are updated to reflect elastic and inelastic collisions. Next, the particle positions and velocities are used to compute the charge density and current density on the mesh. The charge density and current density provide the source terms for the integration of the field equations (Poisson equation in the electrostatic limit, Maxwell's equations in the electromagnetic limit) on the mesh. The fields resulting from the integration are then interpolated to particle locations to provide the force on the particles.

The XOOPIC (X11-based object oriented particle-in-cell)[35] code started as a pioneering effort to apply object oriented techniques to plasma simulation codes. XOOPIC is written in C++, and includes the XGrafix[36] user interface. Applications have ranged from high pressure discharges to relativistic microwave devices. XOOPIC, along with the rest of the suite of plasma device codes developed at University of California at Berkeley, is in use by over one thousand researchers worldwide (including students), with over 70 journal publications and hundreds of conference publications over the last seven years.

XOOPIC models two spatial dimensions in both Cartesian (x,y) and cylindrical (r,z) geometry, including all three velocity components, with both electrostatic and electromagnetic models available. All three components of both the electric and the magnetic fields are modeled, but there is no spatial variation along the ignored coordinate.

XOOPIC uses the message passing interface (MPI)[37] to take advantage of massively parallel, symmetric multiprocessor and distributed architectures, and has demonstrated linear speed up with 16 processors on the Cray T3E. A 3-D version is now under development.[38] This new code is designed around the C++ architecture of the 2-D XOOPIC code. The architecture is extended in four important areas: the advisor, the particle algorithms, the field algorithms and the boundary conditions.

The code presently supports a non-uniform orthogonal mesh and arbitrary placement of most boundary conditions on that mesh. Static magnetic fields can be added

analytically using the equation evaluator, or read from an external file. A number of different charge and current weighting algorithms are available, as well as Poisson and Langdon-Marder divergence corrections for non-conservative current weighting schemes. The code includes a fully relativistic model for inertial particles, as well as a Boltzmann model for inertia-less electrons. Particles and fields can each run on independently subcycled time steps, improving computational efficiency. A temporal filtering scheme reduces high frequency noise, and a spatial digital filtering algorithm reduces short wavelength noise.

XOOPIC also includes volumetric and surface plasma injection, including thermionic and field emission models. Particle statistics can be collected at arbitrary surfaces, and field and particle data can be averaged over arbitrary volumes and surfaces. A Monte Carlo collision (MCC) technique[39] allows multiple background gases at arbitrary partial pressures. The features described are all adjustable from the input file, using MKS (or arbitrary) units for input parameters.

MODIFYING XOOPIC FOR USE IN PLASMA-BASED ACCELERATOR SIMULATIONS

Previous to the work presented here, XOOPIC had never been used for high-energy particle accelerator applications, but had been used extensively to model microwave devices, plasma diodes, plasma display panels, and other low-energy systems, usually in single precision. The authors have modified and enhanced XOOPIC so that it can be used to model high-energy plasma-based accelerators in 2-D Cartesian or cylindrical geometry, in double precision, on the massively parallel Cray T3E. The excellent object-oriented architecture of XOOPIC made it possible to complete this task in a relatively short time.

Development of a Moving Window Algorithm

Plasma-based accelerators are too large to simulate the entire device, and it is only the small region in the vicinity of the particle beam or laser pulse that must be modeled. Because this beam or pulse is moving at the speed of light, it is possible to implement a “moving window” algorithm, such that the simulation follows the small region of interest and ignores the rest of the device.

There are two fundamental approaches to implementing a moving window. One is to move the mathematical mesh along with the particles, and give the background and walls a velocity relative to the mesh. A 3-D moving-window algorithm for cylindrical geometry was implemented in this manner in the ELBA code.[40] The other approach is to keep the mesh stationary with respect to the background, create new particles and fields on the leading edge, shift existing particles and fields to neighboring mesh points, and discard any particles and fields on the trailing edge. The second approach is used for XOOPIC (and also for the OSIRIS code[44]), because it required no modifications to the basic field solve and particle push, and because it eliminates numerous other complications.

For a moving window which is following a group of particles moving to the right, new analytic fields (typically all zero) are introduced into the rightmost row of mesh points, and the fields in the rightmost row of mesh points are copied to the row immediately to the left, and so on. When this shift in the fields takes place, all the particles must also be shifted. At this time, any particles in the leftmost row of cells (for a rightward moving window) are discarded, for they have left the moving window. New particles may be introduced in the rightmost row of cells, if required.

Boundary conditions present no difficulty, if the moving window travels at the speed of light. In the case of a rightward-moving window, disturbances at the leftmost boundary cannot propagate into the moving window, because all electromagnetic waves are constrained to move with a velocity less than or equal to the speed of light. Similarly, incoming fields on the right hand side are not affected by the contents of the moving window to the left, so fields here may be safely specified analytically in a simple way.

Combining parallel operation and the moving window leads to some additional complication. Whenever a shift in fields takes place (usually every time step, or every few time steps), the shifted fields and particles must be passed to the downstream computational region. The moving window in XOOPIC uses MPI to pass particles and fields across computational boundaries, showing linear scaling up to 16 processors on the Cray T3E.

Adding a New Electromagnetic Pulse Launcher

We designed and implemented within XOOPIC the ability to launch a linearly polarized electromagnetic pulse, with a Gaussian time profile and a Gaussian spatial profile along one transverse dimension. The other transverse dimension is along the ignored coordinate, so there is no variation in that direction. The peak intensity, the wavelength and the pulse length can all be specified from the input file, as can the initial divergence or convergence of the pulse.

Implementation within the code was fairly straightforward. We created a new derived class, PortGauss, which inherits from the previously existing boundary class, Port. Due to the benefits of dynamic polymorphism, a PortGauss instance (or object) can be used anywhere in the code as a substitute for the old Port object.

Generalization of the Particle Beam Emitters

The beam emission boundary conditions in XOOPIC have been extended to handle more general cases. Spatial dependence has been added to both the BeamEmitter algorithm, which emits particles of a specified computational particle weight as well as the VarWeightBeamEmitter algorithm, which emits particles of variable weights. Particle weight is defined as the ratio of the charge of a computational particle to that of a physical particle, $w=q_c/q_p$. The particle weight in the VarWeightBeamEmitter has also been generalized to have both spatial and temporal dependence, and the weight can be adjusted automatically to emit a fixed number of particles per time step.

The previously existing emitter models in XOOPIC emitted a specified time-dependent current, I(t), which could be specified from the input file. Only uniform

current density was possible. Furthermore, the VarWeightBeamEmitter only allowed for variation of the weight of particles based on the radial origin of emission for particles, $w(r)=w_{max}r/r_{max}$.

LASER-DRIVEN PLASMA ACCELERATOR SIMULATIONS

We present two simulations of the standard LWFA, one driven by a low ($5.5x10^{16}$ W/cm^2) and the other a high ($3x10^{18}$ W/cm^2) peak intensity laser pulse, both in slab geometry. These simulations have relevance to ongoing LWFA experiments at the l'OASIS laboratory of Lawrence Berkeley National Laboratory.[41,42] To understand the detailed particle trapping mechanisms in these experiments, PIC simulations will be performed with parameters similar to the examples shown in this section.

These results demonstrate the capabilities of XOOPIC. Previously, XOOPIC has been used to model the effects of colliding laser pulses.[43]

Modeling the Wakefield Generated by a Low Intensity Laser Pulse

We first consider the plasma wakefield generated by a low intensity laser pulse. The electron plasma density is $n_e=3x10^{19}$ cm^{-3}, which corresponds to an EPW wavelength of $\lambda_p = 6\,\mu m = 6.2\, c/\omega_p$ and a plasma frequency of $\omega_p=3.1\ x10^{14}$ rad/s.

The laser pulse is linearly polarized, with a transverse Gaussian profile. The minimum laser spot size is $5\ \mu m = 5.2\, c/\omega_p$, and the Rayleigh length is $\lambda_R = 97\ \mu m = 100\ c/\omega_p = 16\ \lambda_p$. In order to maximize the EPW amplitude, the laser pulse length is chosen to be of order λ_p, with a full width at half maximum $\tau_{fwhm} = 6.7$ fs $= 2\ \mu m = \lambda_p/3$. The peak laser intensity is $I_L=5.5x10^{16}$ W/cm^2, corresponding to a dimensionless amplitude $a_0=0.2$, and the laser wavelength is $\lambda=1\ \mu m = 1\ c/\omega_p$.

Figure 1 shows a surface plot of the longitudinal electric field E_x over the mesh. The length of the simulation region is $L_x = 30\ \mu m = 31\ c/\omega_p$ in the x (longitudinal) direction and $L_y = 50\ \mu m = 52\ c/\omega_p$ in the y (transverse) direction. The simulation uses 7 macro-particles per cell to represent the plasma, and the initial plasma is cold.

The plasma wake can be clearly seen behind the laser pulse. The plasma wake is linear, with a peak gradient of $E_x \sim 5.5$ GV/m $\sim 0.01\ E_0$. The peak field of the EPW is significantly smaller than the peak longitudinal field of the laser pulse.

The Wakefield of a High-Intensity Laser Pulse

We now consider the plasma wakefield generated by a high intensity laser pulse. All the physical and simulation parameters are the same as for the low intensity pulse of the previous subsection, but the peak intensity is now $I_L=3x10^{18}$ W/cm^2, corresponding to a dimensionless amplitude $a_0=1.5$.

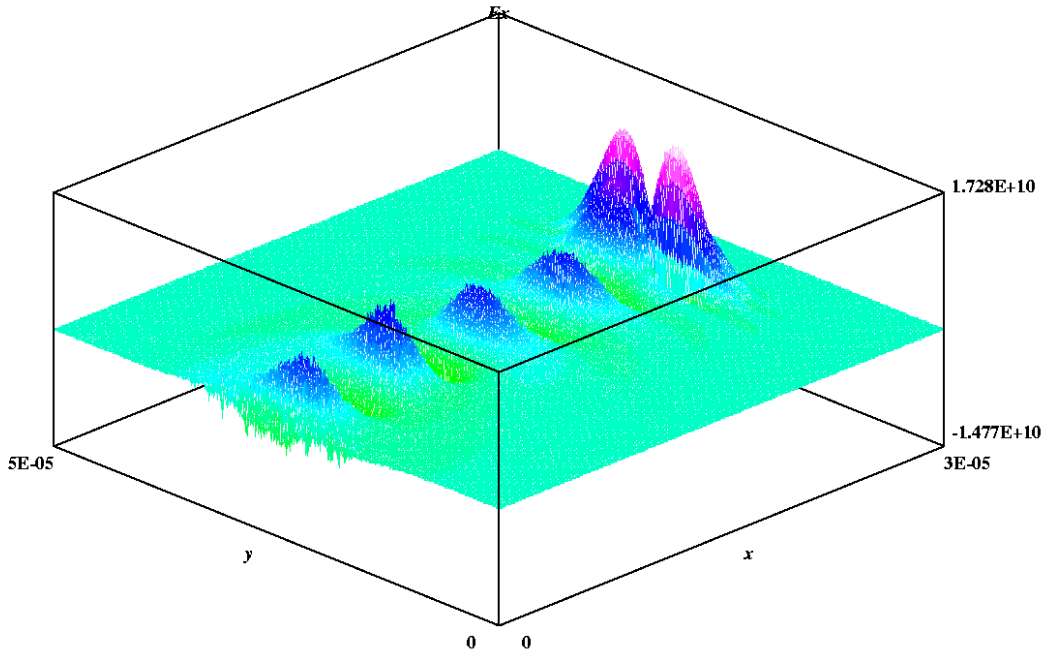


FIGURE 1. Surface plot of the longitudinal electric field generated by the 5.5×10^{16} W/cm^2 (a_0=0.2) laser pulse (large peaks to the right) and the resulting plasma wake (smaller peaks, left and center).

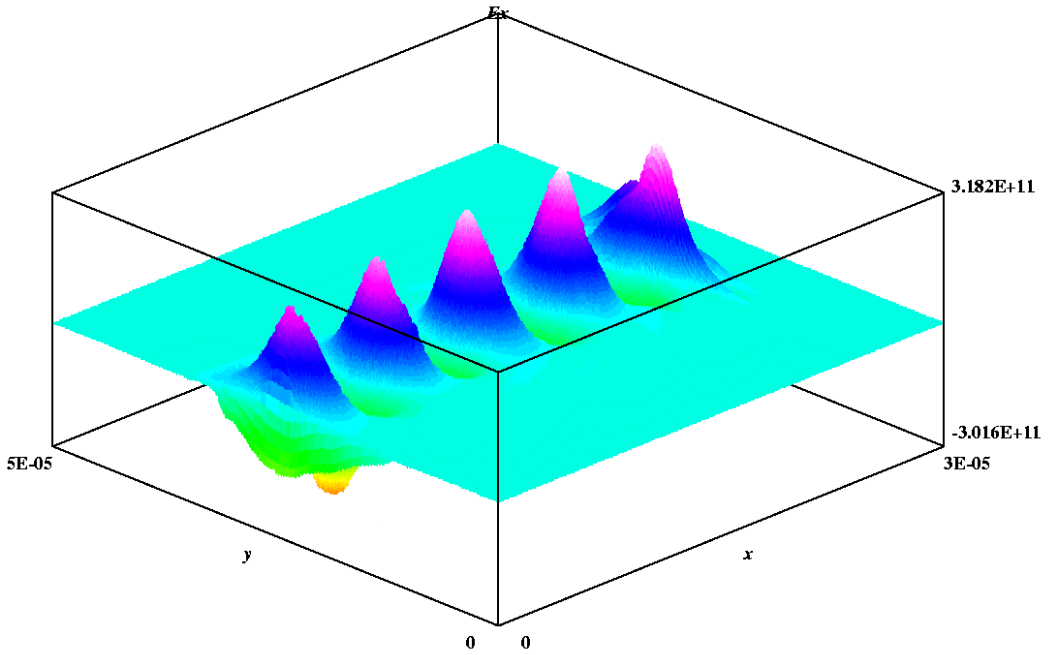


FIGURE 2. Surface plot of the longitudinal electric field generated by the 3×10^{18} W/cm^2 (a_0=1.5) laser pulse (smaller, partially hidden peaks to the far right) and the resulting plasma wake (larger peaks).

Figure 2 shows a surface plot of the longitudinal electric field E_x over the mesh for the high-intensity case. The EPW can be clearly seen behind the laser pulse, but in this case the wake is nonlinear, and has a peak gradient of $E_x \sim 300\,\mathrm{GV/m} \sim 0.56\,E_0$. The wake amplitude is found to increase linearly with the peak laser intensity (as the square of the dimensionless amplitude) when $I_L<3\times10^{18}$ W/cm^2, in agreement with theory.

BEAM-DRIVEN PLASMA ACCELERATOR SIMULATIONS

Here we present some XOOPIC simulations of plasma wakefield acceleration. Our simulations of the E-157 PWFA experiment at SLAC show good agreement with results obtained previously using the OSIRIS[44] code. We also discuss the important issue of electron-neutral collisions.

Modeling the SLAC E-157 Experiment

We have modeled E-157 with XOOPIC and found agreement with previous work.[31,32] The simulation region, in 2-D cylindrical geometry, is 0.9 mm in r by 5.4 mm in z, with the corresponding number of grid points n_r=32 and n_z=192, for a total of 6144 cells. With 4 macro-particles per cell representing the plasma electrons, there are 24,576 plasma particles. The 30 GeV electron beam is represented by 9 macro-particles per cell, and the beam covers 8 by 64 grids (initially) for 4608 beam particles. The grid size is dz=dr=28 μm. The time step, chosen to satisfy the Courant condition, is dt=.5*dz/c=4.69x10^{-14} s. Thus, it requires 71,400 time steps to propagate the beam through the 1 m lithium plasma.

The plasma density is taken to be 2.1x10^{14} cm^{-3}, which implies an electron plasma frequency of ω_p=8.2x10^{11} rad/s. Thus, ω_p*dt=0.04 and the electron plasma frequency is being resolved, which is required for stability in a time-explicit PIC code. The lithium plasma is assumed to be cold, but very little numerical heating is observed, because the moving window algorithm "sweeps" the electrons through at the speed of light.

Figure 3 shows the initial 30 GeV beam in cylindrical coordinates, with r on the vertical axis and z on the horizontal axis, and dimensions in m. Figure 4 shows the plasma wake. The crossing of particle trajectories in the wake indicates highly non-laminar flow, which cannot be modeled with a fluid code. The structure of the wake is independent of the beam radius. Figure 5 shows the accelerating field generated by the wake in V/m. With higher resolution, the peak field on axis is greater than 1 GV/m.

The peak accelerating field overlaps the tail of the beam. Figure 6 shows the resulting acceleration of beam particles after 1m of propagation through the lithium plasma. The vertical axis is $p_z=\gamma v_z$ in units of m/s. These results agree well with previously published work.[31,32]

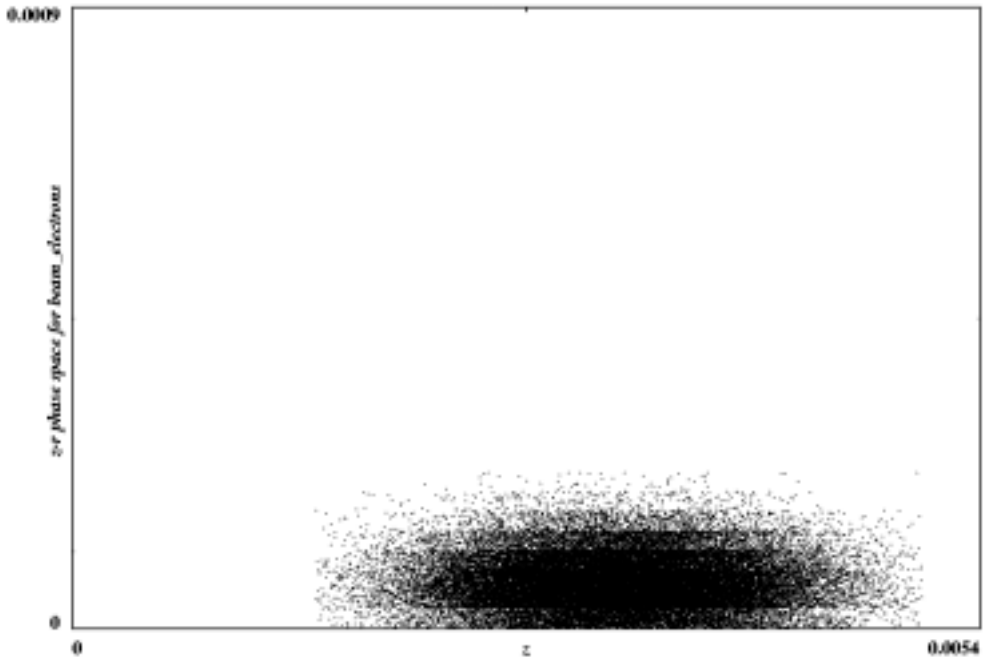


FIGURE 3. Initial distribution of the 30 GeV beam.

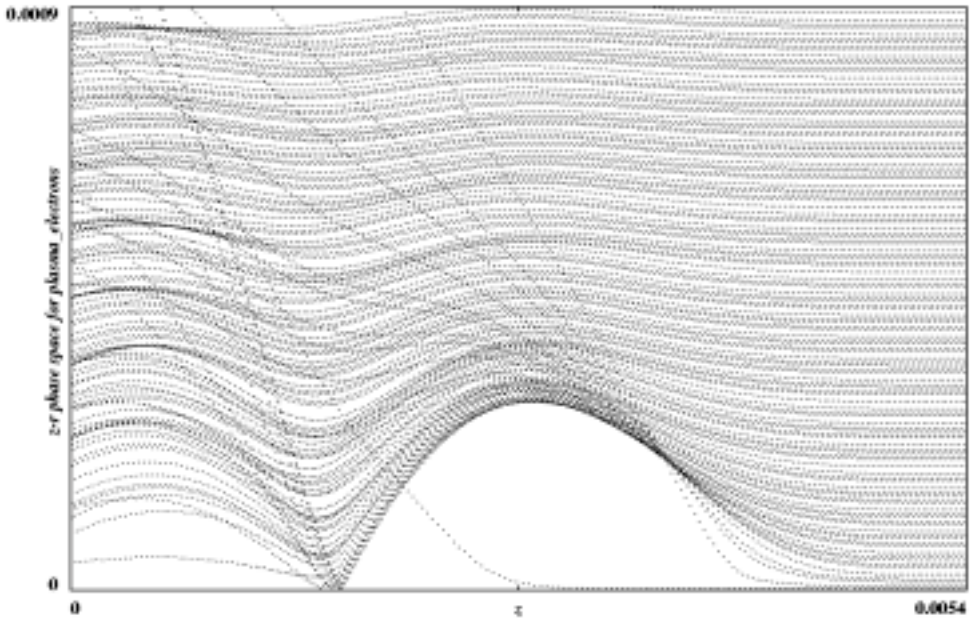


FIGURE 4. Plasma wake.

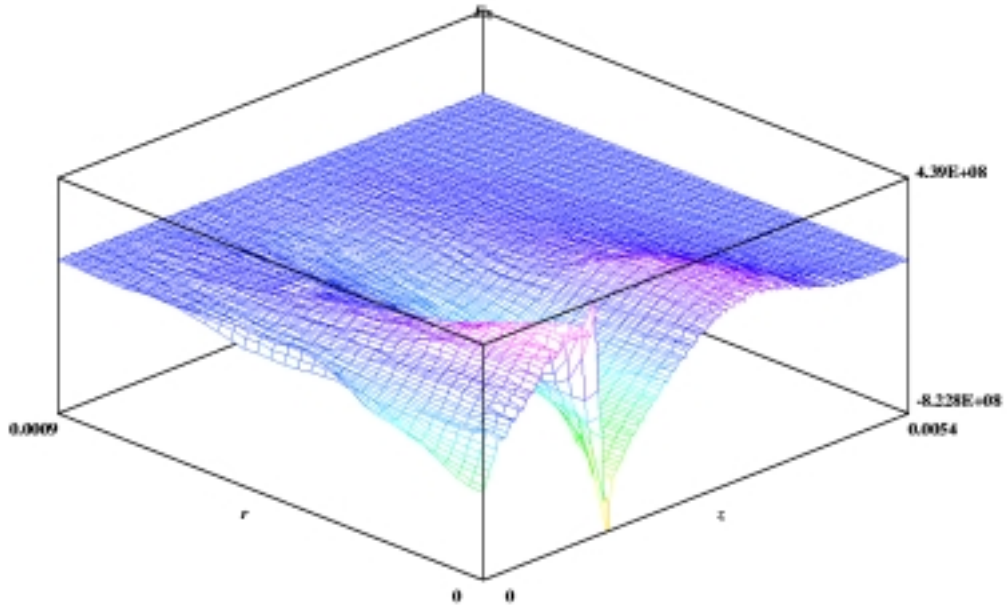


FIGURE 5. Longitudinal electric field.

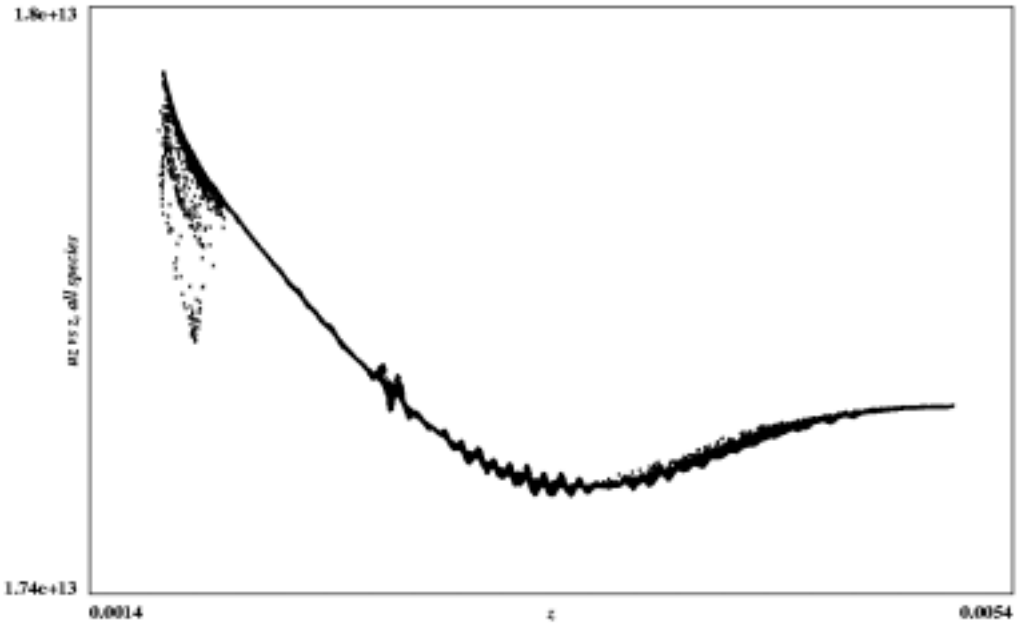


FIGURE 6. z-P_z phase space of beam at 1 m.

Modeling Electron-Neutral Collisions

XOOPIC uses the null collision method[39] for MCC treatment of electron-impact excitation and ionization and for electron-neutral elastic scattering. MCC models for

Ar, Ne, He and H have been used for some time, and we recently added an ionization model for Li, using cross sections from the literature.[45] However, the cross section and scattering models assume the impact energy is nonrelativistic.

The bulk of the plasma electrons in the wake are nonrelativistic for E-157, but a significant fraction are not. Modeling collisional effects involving the drive beam must, of course, be fully relativistic. Electron-neutral collision cross sections $\sigma(E)$ fall from their maximum like $ln(E)/E$ for impact energies E<200KeV.[46,47] Relativistic effects break this scaling, leading to a minimum[48,49] in $\sigma(E)$ for E~1 MeV, followed by logarithmic growth, which eventually saturates at a density dependent energy (the Fermi plateau).[49-52]

A simple fitting function for impact ionization cross sections has been developed,[53] using the ionization energy and two adjustable parameters, approximately capturing both low-energy and relativistic behavior (but not the Fermi plateau). The fitting parameters are determined largely by data for impact energies near 1 MeV, which has been published for a number of gasses[48] (although not lithium). Fitting functions have also been developed for the energy distribution of the secondary electrons,[54-57] and there is some applicable theory in certain regimes.[58-60] Several works discuss the angular distribution for elastic and inelastic scattering in relativistic and nonrelativistic regimes.[50,56,57,60-62] We are presently compiling new and comprehensive parametric models for impact ionization and elastic scattering for a wide range of energies, to be published elsewhere.

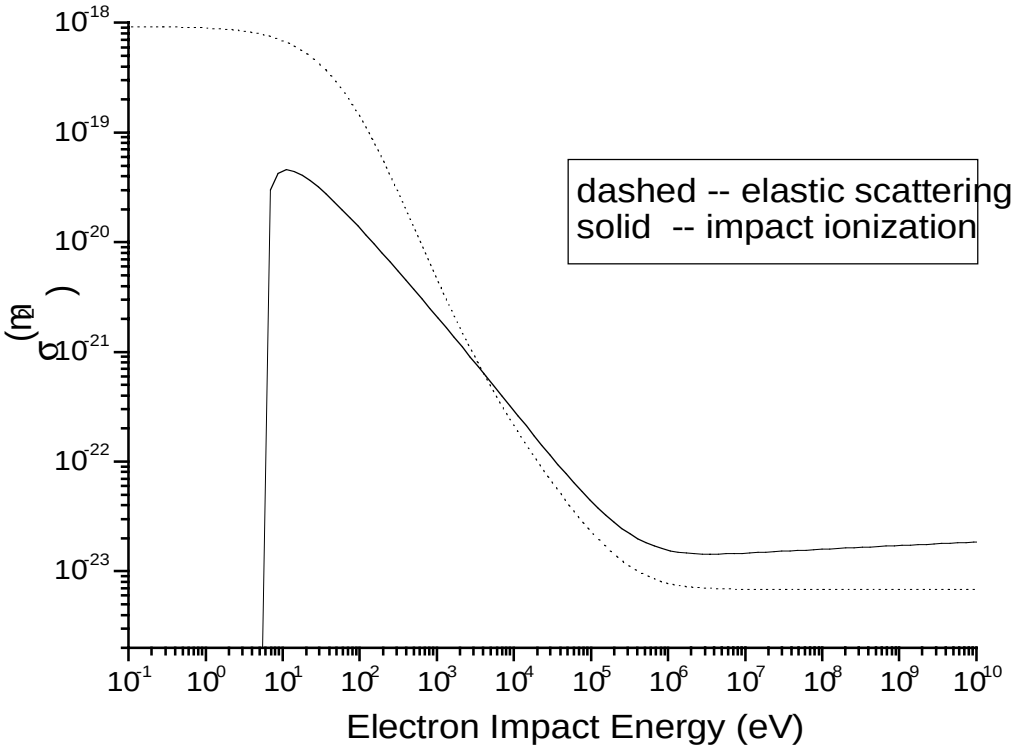


FIGURE 7. Total cross sections (in m^2) for electron collisions with neutral lithium, as a function of impact energy (1 m^2 = 10^4 cm^2 = 10^{28} barns). The dashed line is for elastic scattering and the solid line is for impact ionization. These lines are parametric fits to previously published results.

Figure 7 shows parametric fits to electron-impact cross-sections for lithium, for an energy range of 0.1 eV < E < 10 GeV. The solid line is for ionization of neutral lithium (ejecting the outer electron from the 2s shell). The dashed line is for elastic scattering. The fitting parameters for ionization were determined from Ref. 45 (low energy) and Ref. 63 (high energy). The fitting parameters for elastic scattering were determined from Ref. 64 (low energy) and Ref. 63 (high energy). We note that the cross section for elastic scattering is orders of magnitude larger than the ionization cross section at low energies.

We have conducted some simulations using a nonrelativistic impact ionization model for lithium.[65] The neutral lithium background density is assumed to be ten times the plasma density, which corresponds to 2×10^{15} cm^{-3} for E-157. Impact ionization is found to be negligible for E-157. We also modeled the case where the lithium density is larger by a factor of 100 than the density for E-157 (parameters similar to those for the recently proposed afterburner concept[28]). Simulations indicate that impact ionization is not completely negligible for this higher density, but that the plasma wake and corresponding accelerating fields are not significantly modified. However, the electron-neutral scattering cross section is much larger, and this scattering might disrupt the wake, even for neutral lithium densities of order 10^{17} cm^{-3}. A detailed study of these effects is the subject of a future publication.

SUMMARY

The code XOOPIC has been modified to enable simulations of plasma based accelerators on massively parallel platforms. Modifications include the development of a moving window algorithm, adding a new electromagnetic pulse launcher, generalization of the particle beam emitters, and further optimization to allow efficient use on parallel platforms. As examples of the utility of XOOPIC, simulations of the standard LWFA with both low and high intensity laser pulses were performed, and the results were in agreement with the theoretically predicted wake amplitudes. In addition, simulations of the PWFA were preformed. Simulations for the parameters of the E-157 experiment were found to be in agreement with previous studies. Simulations using the nonrelativistic impact ionization model for lithium indicated insignificant effects for the parameters of E-157. However, electron-neutral scattering could possibly alter the wake for neutral lithium densities of order 10^{17} cm^{-3} or higher.

ACKNOWLEDGMENTS

The authors gratefully acknowledge many helpful and interesting conversations with C.K. Birdsall, P. Chen, R. Hemker, R. Hubbard, C. Joshi, T. Katsouleas, W. Mori, J. Ng and F. Tsung. This work is supported by the U.S. Department of Energy, under Contract No.'s DE-FG03-99ER82903, DE-FG03-95ER40926 and DE-AC03-76SF00098, and by Tech-X Corporation. This research used resources of the National Energy Research Scientific Computing Center, which is supported by the Office of Science of the U.S. Department of Energy under Contract No. DE-AC03-76SF00098.

REFERENCES

1. Esarey, E., et al., IEEE Trans. Plasma Science **24**, 252 (1996).
2. Umstadter, D., et al., Phys. Rev. Lett. **76**, 2073 (1996).
3. Hemker, R.G., et al., Phys. Rev. Lett. **57**, 5920 (1998).
4. Esarey, E., Hubbard, R.F., Leemans, W.P., et al., Phys. Rev. Lett. **79**, 2682 (1997).
5. Schroeder, C.B., et al., Phys. Rev. E **59**, 6037 (1999).
6. Esarey, E., Schroeder, C.B., Leemans, W.P., and Hafizi, B., Phys. Plasmas **6**, 2262 (1999).
7. Moore, C.I., et al., Phys. Rev. Lett. **82**, 1688 (1999).
8. Duda, B.J., Hemker, R.G., Tzeng, K.C., and Mori, W.B., Phys. Rev. Lett. **83**, 1978 (1999).
9. Andreev, N.E., et al., Phys. Rev. Special Topics -- Accelerators and Beams **3**, 021301 (2000).
10. Modena, A., Najmudin, Z., Dangor, A.E., *et al.*, Nature **377**, 606 (1995).
11. Nakajima, K., Fisher, D., Kawakubo, T., *et al.*, Phys. Rev. Lett. **74**, 4428 (1995).
12. Coverdale, C., Darrow, C.B., Decker, C.D., *et al.*, Phys. Rev. Lett. **74**, 4659 (1995).
13. Wagner, R., Chen, S.Y., Maksimchuk, A., and Umstadter, D., Phys. Rev. Lett. **78**, 3125 (1997).
14. Ting, A., Moore, C.I., Krushelnick, K., *et al.*, Phys. Plasmas **4**, 1889 (1997).
15. Gordon, D., Tzeng, K.C., Clayton, C.E., *et al.*, Phys. Rev. Lett. **80**, 2133 (1998).
16. Volfbeyn, P. , Esarey, E., and Leemans, W.P., Phys. Plasmas **6**, 2269 (1999).
17. Decker, C.D., Mori, W.B., and Katsouleas, T., Phys. Rev. E **50**, R3338 (1994).
18. Decker, C.D., Mori, W.B., Tzeng, K.C., and Katsouleas, T., Phys. Plasmas **3**, 2047 (1996).
19. Bulanov, S.V., et al., Phys. Fluids B **4**, 1935 (1992).
20. Bulanov, S.V., Pegoraro, F., and Pukhov, A.M., Phys. Rev. Lett. **74**, 710 (1995).
21. Andreev, N.E., et al., JETP Letters **55**, 571 (1992).
22. Krall, J., Ting, A., Esarey, E., and Sprangle, P., Phys. Rev. E **48**, 2157 (1993).
23. Antonsen, T.M., and Mora, P., Phys. Fluids B **5**, 1440 (1993).
24. Mora, P., and Antonsen, T.M., Phys. Plasmas **4**, 217 (1997).
25. Sprangle, P., Esarey, E., and Ting, A., Phys. Rev. Lett. **64**, 2011 (1990).
26. Chen, P., Dawson, J., Huff, R. and Katsouleas, T., Phys. Rev. Lett. **54**, 693 (1985).
27. Ruth, R., Chao, A., Morton, P., and Wilson, P., Part. Accel. **17**, 171 (1985).
28. Katsouleas, T., *et al*., these proceedings.
29. Assmann, R. *et al*., in *Proc. 1999 Particle Accelerator Conference* (IEEE, NY, 1999), p. 130.
30. Muggli, P., et al., in *Proc. 1999 Particle Accelerator Conference* (IEEE, NY, 1999), pp. 3651-3653.
31. Lee, S., et al., Phys. Rev. E **61**, 7014 (2000)
32. Hogan, M.J., et al., Phys. Plasmas **7**, 2241-2248 (2000).
33. SLAC E-157 web site, URL http://www.slac.stanford.edu/grp/arb/e157
34. Birdsall, C.K., and Langdon, A.B., *Plasma Physics via Computer Simulation*, New York: McGraw-Hill, 1985.
35. Verboncoeur, J.P., Langdon, A.B., and Gladd, N.T., Comp. Phys. Comm. **87**, 199-211 (1995).
36. Vahedi, V., Verboncoeur, J.P., and Birdsall, C.K., "XGrafix: an X-Windows Environment for Real-Time Interactive Simulations," Proc. 14th Conf. on the Numerical Simulation of Plasmas, 1991.
37. The MPI home page at URL http://www.mcs.anl.gov/mpi .
38. Mardahl, P., and Verboncoeur, J.P., IEEE Intl. Conf. Plasma Science, (Monterey, CA, June 1999).
39. Vahedi, V., and Surendra, M., Computer Phys. Comm. **87**, 179-198 (1995).
40. Joyce, G., Krall, J., and Slinker, S., Laser and Particle Beams **12**, 273-282 (1994).
41. Leemans, W.P., *et al.*, Phys. Plasmas **5**, 1615 (1998).
42. Leemans, W.P., *et al.*, these proceedings.
43. Giacone, R.E., Cary, J.R., Bruhwiler, D.L., Mardahl, P., and Verboncoeur, J.P., *Proc. Seventh European Particle Accelerator Conference*, (Vienna, June, 2000), pp. 907-909.
44. Hemker, R.G., et al., in *Proc. 1999 Particle Accelerator Conf.* (IEEE, NY, 1999), pp. 3672-3674.
45. Younger, S.M., Journal of Quantum Spectroscopy and Radiative Transfer **26**, 329 (1981).
46. Younger, S.M., and Märk, T.D., in *Electron Impact Ionization*, edited by T.D. Märk and G.H. Dunn, Vienna: Springer-Verlag, 1985, pp. 24-41.

47. Brown, S.C., *Basic Data of Plasma Physics, The Fundamental Data on Electrical Discharges in Gases*, New York: American Institute of Physics, 1994.
48. Rieke, F.F., and Prepejchal, W., Phys. Rev. A **6**, 1507 (1972).
49. Jackson, J.D., *Classical Electrodynamics*, 2nd Edition, New York: Wiley, 1975, pp. 618-653.
50. Fermi, E., Phys. Rev. **57**, 485-493, 1940.
51. Rossi, B., *High-Energy Particles*, New York: Prentice Hall, 1952, pp. 27-29.
52. Cobb, J.H., Allison, W.W.M., and Bunch, J.N., Nucl. Instrum. and Meth. **133**, 315-323 (1976).
53. Reiser, M., *Theory and Design of Charged Particle Beams*, New York: Wiley, 1994, pp. 273-278.
54. Opal, C.B., Peterson, W.K., and Beatty, E.C., J. Chem. Phys. **55**, 4100 (1971).
55. Slinker, S.P., Taylor, R.D., and Ali, A.W., J. Appl. Phys. **63**, 1 (1988).
56. Rudd, M.E., Phys. Rev. A **44**, 1644 (1991).
57. Rudd, M.E., *et al.*, Phys. Rev. A **47**, 1866 (1993).
58. Moeller, C., Annalen der Physik 14, 531-585 (1932).
59. Bethe, H.A., and Ashkin, J., in *Experimental Nuclear Physics*, Vol. 1, edited by E. Segrè, New York: John Wiley & Sons, 1953, pp. 166-357.
60. Kalinovskii, A.N., Mokhov, N.V., and Nikitin, Y.P., *Passage of High-Energy Particles through Matter*, New York: American Institute of Physics, 1989, pp. 29-54.
61. Mott, N.F., and Massey, H.S.W., *The Theory of Atomic Collisions*, 2nd Edition, Oxford: Oxford University Press, 1949.
62. Goldstein, H., *Classical Mechanics*, 2nd Edition, Reading: Addison-Wesley, 1980, pp. 309-320.
63. Perkins, S.T., Cullen, D.E., and Seltzer, S.M., Lawrence Livermore National Laboratory report UCRL-50400, Vol. **31** (1991).
64. Bray, I., Fursa, D.V., and McCarthy, I.E., Phys. Rev. A **47**, 1101-1110 (1993).
65. Bruhwiler, D.L., Cary, J.R., Verboncoeur, J.P., Mardahl, P., and Giacone, R., *Proc. Seventh European Particle Accelerator Conference*, (Vienna, June, 2000), pp. 877-879.